The Application of the Semigeostrophic Equations to the Frontal Instability Problem

DEAN G. DUFFY[1]

AFGWC/WPA, Offutt AFB, Nebr. 68113

(Manuscript received 17 May 1976, in revised form 9 August 1976)

ABSTRACT

The stability of the classical Norwegian polar front model is reinvestigated, using a numerical technique to supplement the precise conclusions which are possible in the limiting case of zero density difference or zero wavenumber. Instead of using the primitive equations, a system of filtered momentum equations which neglects the substantial derivative of the ageostrophic part of the horizontal wind is used to test the applicability to meteorological problems. For Rossby numbers $\leqslant 0.4$, the agreement between the primitive and the semigeostrophic equations is found to be good provided that the Richardson number is not too small. Unstable waves are found only at Rossby numbers less than a critical value; large-scale shear instability exists at small Richardson number and quasigeostrophic baroclinic instability occurs at larger Richardson number.

1. Introduction

For the study of complex atmospheric processes, the use of the primitive equations often results in little physical insight due to the fact that these equations are so general. In addition, the numerical integration of these equations is sensitive to the computational methods used. Consequently, meteorologists have sought simplified forms of the primitive equations which neglect or filter out meteorologically unimportant phenomena. Of those in popular use, the simplest is the barotropic vorticity equation, followed in complexity by the quasigeostrophic equations and finally the balance equations.

Recently Hoskins (1975) has suggested that we add to our list a system of hydrostatic, filtered, Boussinesq momentum equations, first derived by Eliassen (1949), which neglects the substantial derivative of the ageostrophic part of the horizontal wind. Since the total horizontal wind (i.e., the geostrophic plus the ageostrophic part of the horizontal wind) is retained in the advection terms of the substantial derivative, this system can be referred to as the "semigeostrophic equations."

Through the use of a coordinate transformation, Hoskins showed that these approximate momentum equations, along with the continuity and thermodynamic equations, are equivalent to a system which is very similar in mathematical form to that of the quasigeostrophic equations.[2] Due to the simplicity of these transformed semigeostrophic equations, Hoskins has suggested that these equations might be useful in the analytic and numerical analysis of ageostrophic phenomena. To demonstrate this, Hoskins and Bretherton (1972) and Hoskins (1975), respectively, have examined frontogenesis and nonlinear baroclinic instability using this form of the semigeostrophic equations. Most recently, Hoskins (1976) has used the semigeostrophic equations to study the development into the nonlinear regime of the Eady wave instability mode of a zonal flow with uniform shear in the vertical.

Despite the aforementioned applications of the semigeostrophic equations, these equations have been ignored in general since their derivation in 1949. Consequently, little is known about the properties of this system of approximate momentum equations and widespread acceptance will only come after this system has been more thoroughly tested than to date.

It is the intention of this paper to study the instability of frontal waves using the semigeostrophic equations. We have chosen this problem for several reasons.

As a meteorological problem, it has been exhaustively studied, having been solved without approximation by Orlanski (1968). From Orlanski's study, the solutions are well known for a wide variety of Rossby and Richardson numbers and the dynamics are generally understood. Consequently, it is an ideal problem for the testing of systems of equations which approximate the hydrostatic Boussinesq equations. This is especially true for the semigeostrophic equations since we will not have to contend with any coordinate transforma-

[1] 1st Lt., U. S. Air Force.

[2] Hoskins refers to these transformed equations as the semigeostrophic equations.

tions, as did Hoskins and Bretherton, in order to obtain the solutions.

In testing equations which are to approximate the primitive equations, care must be taken not to contrive a test flow which satisfies both the primitive equations and the approximate system of equations. Upon examining the solutions found by Orlanski, it is found that only in the limit of vanishing Rossby number, where the flow becomes quasigeostrophic, will the solutions to the primitive and semigeostrophic equations be the same.

Finally, the semi-geostrophic equations have been suggested for use in numerical weather prediction (see Hoskins, 1975). These equations should be able to capture the fundamental physics associated with frontal cyclogenesis. If they do not, then their usefulness in numerical weather prediction would be dubious.

For these reasons we shall reexamine the stability of a Margules frontal surface to perturbation. We shall use the semigeostrophic equations, which will be derived for this two-fluid system in Section 2, instead of the primitive equations.

To facilitate comparison between our results and Orlanski's we shall pattern our sections after his arrangement. Consequently, the basic state will be derived in Section 3, the perturbation equations will be derived in Section 4, shear waves will be studied in Section 5 and the instability of very long waves will be examined in Section 6. We shall discuss the most general case in Section 7 with kinematics and energetics in Sections 8 and 9. We will discuss our findings in Section 10.

2. The governing equations

We consider two layers of incompressible homogeneous fluid in a rotating coordinate system with constant Coriolis parameter f. The motion in each layer is hydrostatic and independent of the vertical coordinate z^*, and the two fluids are bounded above and below by rigid horizontal planes at $z^*=0$ and H. The interface between the layers is at $z^*=h(x,y,t)$, where $0\leqslant h\leqslant H$.

Let $\mathbf{k}$ be the vertical unit vector, ∇^* the horizontal gradient operator, and $\mathbf{v}_j^*$ the horizontal wind vector, with components u_j^* and v_j^*, in either the lower ($j=1$) or upper ($j=2$) layer. Pressures p_1^* and p_2^* are given at $z^*=0$ and $z^*=H$, respectively. The governing equations for this model, which satisfy the dynamic and kinematic conditions at $z^*=0$, h and H, are as follows:

$$\left[\frac{\partial}{\partial t^*}+(\mathbf{v}_j^*\cdot\nabla^*)+f\mathbf{k}\times\right]\mathbf{v}_j^*=-\frac{1}{\bar{\rho}}\nabla^* p_j^*, \tag{2.1}$$

$$p_1^*=p_2^*+(\rho_1-\rho_2)gh^*+\rho_2 gH, \tag{2.2}$$

$$\frac{\partial h^*}{\partial t^*}=-\nabla^*\cdot(h^*\mathbf{v}_1^*)=\nabla^*\cdot(H-h^*)\mathbf{v}_2^*, \tag{2.3}$$

where $\rho_1\geqslant\rho_2$. We have also invoked the Boussinesq approximation by replacing ρ_j in the pressure term of (2.1) by $\bar{\rho}=\frac{1}{2}(\rho_1+\rho_2)$.

To nondimensionalize (2.1)–(2.3) we define nondimensional independent variables as follows:

$$x=kx^*,\quad y=ky^*/\mathrm{RiRo},\quad z=z^*/H,$$
$$\mathbf{v}_j=\mathbf{v}_j^*/\bar{U},\quad t=k\bar{U}t^*,\quad p_1=p_1^*k/\bar{\rho}f\bar{U},$$
$$p_2=k(p_2^*+\rho_2 gH)/\bar{\rho}f\bar{U}\quad\text{and}\quad h=(\rho_1-\rho_2)gkh^*/\bar{\rho}f\bar{U}.$$

For the present k^{-1} and $\bar{U}$ are length and velocity scales which will take on specific physical interpretations as the analysis proceeds, $\mathrm{Ro}=k\bar{U}/f$ and

$$\mathrm{Ri}=gH(\rho_1-\rho_2)/4\bar{U}^2\bar{\rho}.$$

The nondimensional form of (2.1)–(2.3) now becomes

$$\mathrm{Ro}\left(\frac{\partial}{\partial t}+\mathbf{v}_j\cdot\nabla\right)\mathbf{v}_j+\mathbf{k}\times\mathbf{v}_j=-\nabla p_j, \tag{2.4}$$

$$h=p_1-p_2 \tag{2.5}$$

$$\frac{\partial h}{\partial t}=-\nabla\cdot(h\mathbf{v}_1)=\nabla\cdot[(4\,\mathrm{RiRo}-h)\mathbf{v}_2], \tag{2.6}$$

where $\nabla=(\partial/\partial x,\partial/\mathrm{RiRo}\partial y)$.

Concentrating on (2.4) for the moment and omitting the subscripts, we may rewrite (2.4) as

$$v=\frac{\partial p}{\partial x}+\mathrm{Ro}\left(\frac{\partial}{\partial t}+\mathbf{v}\cdot\nabla\right)u, \tag{2.7}$$

$$u=-\frac{1}{\mathrm{RiRo}}\frac{\partial p}{\partial y}-\mathrm{Ro}\left(\frac{\partial}{\partial t}+\mathbf{v}\cdot\nabla\right)v. \tag{2.8}$$

We now substitute (2.8) into the substantial derivative in (2.7) and substitute (2.7) into the substantial derivative in (2.8) in such a manner as to obtain

$$v=\frac{\partial p}{\partial x}-\frac{1}{\mathrm{Ri}}\frac{D}{Dt}\left(\frac{\partial p}{\partial y}\right)-\mathrm{Ro}^2\frac{D^2 v}{Dt^2}, \tag{2.9}$$

$$u=-\frac{1}{\mathrm{RiRo}}\frac{\partial p}{\partial y}-\mathrm{Ro}\frac{D}{Dt}\left(\frac{\partial p}{\partial x}\right)-\mathrm{Ro}^2\frac{D^2 u}{Dt^2}, \tag{2.10}$$

where $D/Dt=\partial/\partial t+\mathbf{v}\cdot\nabla$. Upon repeated substitution of (2.7)–(2.8) into the substantial derivative (in the same manner as above) to replace v and u, respectively, we may replace (2.7)–(2.8) with the power series

$$v=\sum_{n=0}^{\infty}(-1)^n\,\mathrm{Ro}^{2n}\frac{D^{2n}}{Dt^{2n}}\left[\frac{\partial p}{\partial x}-\frac{1}{\mathrm{Ri}}\frac{D}{Dt}\left(\frac{\partial p}{\partial y}\right)\right], \tag{2.11}$$

$$u=\sum_{n=0}^{\infty}(-1)^n\,\mathrm{Ro}^{2n}\frac{D^{2n}}{Dt^{2n}}\times\left[-\frac{1}{\mathrm{RiRo}}\frac{\partial p}{\partial y}-\mathrm{Ro}\frac{D}{Dt}\left(\frac{\partial p}{\partial x}\right)\right]. \tag{2.12}$$

The semigeostrophic equations result when (2.11)–(2.12) are truncated at $n=0$:

$$-\frac{1}{\mathrm{Ri}}\frac{D}{Dt}\left(\frac{\partial p}{\partial y}\right)+\frac{\partial p}{\partial x}-v=0, \tag{2.13}$$

$$\mathrm{Ro}\frac{D}{Dt}\left(\frac{\partial p}{\partial x}\right)+\frac{1}{\mathrm{RiRo}}\frac{\partial p}{\partial y}+u=0. \tag{2.14}$$

Eqs. (2.13)–(2.14) will be good approximations to (2.7)–(2.8) if, upon solving (2.13)–(2.14) along with (2.5)–(2.6) to obtain p, u and v for a given Ro and Ri, it is found that the remaining terms of (2.11)–(2.12) are small compared to the $n=0$ term.

Certainly for small Rossby number it will be found that for most of the flow field the $n=0$ term greatly dominates over the neglected terms. There will be, however, small regions in which the $n=0$ term vanishes so that the neglected terms may be larger than the $n=0$ term. This would indicate that the semigeostrophic equations are giving locally poor results, but the remaining portions of the flow field are described very accurately. Consequently, in testing the validity of the semigeostrophic equations to the whole flow field, a global view of whether the neglected terms are small compared to the $n=0$ term is needed.

As we increase the magnitude of the Rossby number, the regions where the neglected terms become comparable to or larger than the $n=0$ term become larger and larger until most of the flow field can no longer be described using the semigeostrophic equations. At that point, we must resort to using the primitive equations or a set of approximate momentum equations which include higher order terms in the Taylor expansions (2.11)–(2.12) if we wish to continue the analysis.

In this paper, instead of computing the neglected terms for a given Ro and Ri, it is far more convenient to directly compare our results using the semigeostrophic equations with Orlanski's results from the primitive equations. In particular, we will compare the complex phase speeds found in this paper with those found in Orlanski's paper.

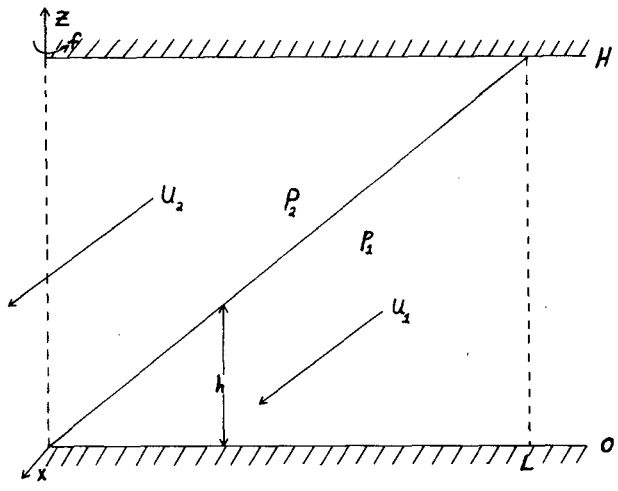

FIG. 1. Frontal surface model.

Replacing (2.4) with the semigeostrophic equations (2.13)–(2.14), we replace (2.4)–(2.6) with

$$\mathrm{Ro}\left(\frac{\partial}{\partial t}+\mathbf{v}_j\cdot\nabla\right)(\mathbf{k}\times\nabla p_j)+\mathbf{k}\times\mathbf{v}_j=-\nabla p_j, \tag{2.15}$$

$$h=p_1-p_2, \tag{2.16}$$

$$\frac{\partial h}{\partial t}=-\nabla\cdot(h\mathbf{v}_1)=\nabla\cdot[(4\,\mathrm{RiRo}-h)\mathbf{v}_2]. \tag{2.17}$$

By forming a vorticity equation, (2.15)–(2.17) may be replaced by

$$h\left(\frac{\partial}{\partial t}+u_1\frac{\partial}{\partial x}+v_1\frac{1}{\mathrm{RiRo}}\frac{\partial}{\partial y}\right)\zeta_1 -\zeta_1\left(\frac{\partial}{\partial t}+u_1\frac{\partial}{\partial x}+\frac{v_1}{\mathrm{RiRo}}\frac{\partial}{\partial y}\right)h=0, \tag{2.18}$$

$$(4\,\mathrm{RiRo}-h)\left(\frac{\partial}{\partial t}+u_2\frac{\partial}{\partial x}+\frac{v_2}{\mathrm{RiRo}}\frac{\partial}{\partial y}\right)\zeta_2 +\zeta_2\left(\frac{\partial}{\partial t}+u_2\frac{\partial}{\partial x}+\frac{v_2}{\mathrm{RiRo}}\frac{\partial}{\partial y}\right)h=0, \tag{2.19}$$

where

$$\zeta_i=1+\mathrm{Ro}\left(\frac{\partial^2 p_i}{\partial x^2}+\frac{1}{\mathrm{Ri}^2\mathrm{Ro}^2}\frac{\partial^2 p_i}{\partial y^2}\right) -\frac{1}{\mathrm{Ri}^2}\left(\frac{\partial^2 p_i{}^2}{\partial x\partial y}\right)+\frac{1}{\mathrm{Ri}^2}\frac{\partial^2 p_i}{\partial x^2}\frac{\partial^2 p_i}{\partial y^2}.$$

We shall use (2.18)–(2.19) for the analysis which is to follow.

3. The basic state

The basic state consists of a uniform velocity U_i in the positive x direction in each layer (see Fig. 1). From the semigeostrophic equation (2.15), we find that

$$\frac{d\bar{p}_1}{dy}=-\mathrm{RiRo}\frac{U_1}{\bar{U}}, \tag{3.1}$$

$$\frac{d\bar{p}_2}{dy}=-\mathrm{RiRo}\frac{U_2}{\bar{U}}, \tag{3.2}$$

$$\bar{h}=2\,\mathrm{RiRo}y, \tag{3.3}$$

where the bar over the dependent variables refers to basic-state quantities and $\bar{U}$ has now been defined as $\frac{1}{2}(U_2-U_1)$.

In conformity with Orlanski's analysis, we have the origin of y where the unperturbed frontal surface intersects $z=0$.

4. Perturbation equations

Continuing along the lines of classical hydrodynamic stability theory, we allow the steady flow described above to be perturbed by a wave-like disturbance of infinitesimal amplitude, i.e.,

$$\left.\begin{aligned} u_j &= U_j/\bar{U}+u_j' \\ v_j &= \quad\ v_j' \\ p_j &= \bar{p}_j \quad +p_j' \\ \zeta_j &= 1 \quad\ +\zeta_j' \\ h &= \bar{h} \quad +h' \end{aligned}\right\}. \tag{4.1}$$

The basic-state dependent variables $\bar{p}_j$ and $\bar{h}$, as well as $U_j/\bar{U}$, are defined in the previous section.

We shall assume that each of the perturbed quantities may be expressed in the form

$$(u_j,v_j,p_j,\zeta_j,h)=\mathrm{Re}\left\{\mathcal{U}_j,\ \mathcal{V}_j,\ \mathcal{P}_j,\ \mathcal{Z}_j,\ \mathcal{H}\right. \times\exp\left[ix+i\tau t-\frac{i}{2}\left(\frac{U_1+U_2}{\bar{U}}\right)t\right]\Bigg\}, \tag{4.2}$$

where the script variables are in general a complex function of y and τ is the negative of the nondimensional phase velocity relative to the mean flow. It should be noted that the results obtained from the succeeding analysis will be valid for perturbations with zonal wavenumber k.

Substituting (4.1)–(4.2) into (2.18)–(2.19) and linearizing, we have

$$y\left(\frac{d^2\mathcal{P}_1}{dy^2}-\mathrm{Ri}^2\mathrm{Ro}^2\mathcal{P}_1\right)+\frac{d\mathcal{P}_1}{dy}-\frac{\mathrm{Ri}}{\tau-1}\mathcal{P}_1 =\tfrac{1}{2}\,\mathrm{Ri}(\mathcal{P}_1-\mathcal{P}_2), \tag{4.3}$$

$$(y-2)\left(\frac{d^2\mathcal{P}_2}{dy^2}-\mathrm{Ri}^2\mathrm{Ro}^2\mathcal{P}_2\right)+\frac{d\mathcal{P}_2}{dy}-\frac{\mathrm{Ri}}{\tau+1}\mathcal{P}_2 =\tfrac{1}{2}\,\mathrm{Ri}(\mathcal{P}_1-\mathcal{P}_2), \tag{4.4}$$

$$\mathcal{H}=\mathcal{P}_1-\mathcal{P}_2, \tag{4.5}$$

since

$$\mathcal{V}_1=i\mathcal{P}_1-\frac{i}{\mathrm{Ri}}(\tau-1)\frac{d\mathcal{P}_1}{dy}, \tag{4.6}$$

$$\mathcal{V}_2=i\mathcal{P}_2-\frac{i}{\mathrm{Ri}}(\tau+1)\frac{d\mathcal{P}_2}{dy}. \tag{4.7}$$

Upon making the substitution $y=\eta+1$, we obtain the perturbation equations which most closely correspond to Orlanski's (5.3)–(5.4), i.e.,

$$(\eta+1)\left(\frac{d^2\mathcal{P}_1}{d\eta^2}-\mathrm{Ri}^2\mathrm{Ro}^2\mathcal{P}_1\right)+\frac{d\mathcal{P}_1}{d\eta}-\frac{\mathrm{Ri}}{\tau-1}\mathcal{P}_1 =\tfrac{1}{2}\,\mathrm{Ri}(\mathcal{P}_1-\mathcal{P}_2), \tag{4.8}$$

$$(\eta-1)\left(\frac{d^2\mathcal{P}_2}{d\eta^2}-\mathrm{Ri}^2\mathrm{Ro}^2\mathcal{P}_2\right)+\frac{d\mathcal{P}_2}{d\eta}-\frac{\mathrm{Ri}}{\tau+1}\mathcal{P}_2 =\tfrac{1}{2}\,\mathrm{Ri}(\mathcal{P}_1-\mathcal{P}_2). \tag{4.9}$$

Eqs. (4.8)–(4.9) are identical to Orlanski's (5.3)–(5.4), except for the neglect of $\mathrm{Ro}^2\mathrm{Ri}(\tau-1)^2(\mathcal{P}_1-\mathcal{P}_2)/2$ and $\mathrm{Ro}^2\mathrm{Ri}(\tau+1)^2(\mathcal{P}_1-\mathcal{P}_2)/2$ in (4.8)–(4.9), respectively. Consequently we expect the best agreement between our results and Orlanski's results when $\mathrm{Ro}^2\ll 1$.

It is readily shown that our boundary conditions are nearly identical to Orlanski's, i.e.,

$$\left.\begin{aligned} &\frac{d\mathcal{P}_1}{d\eta}+\mathrm{RiRo}\mathcal{P}_1=0 \\ &\frac{d\mathcal{P}_2}{d\eta}-\frac{\mathrm{Ri}}{\tau+1}\mathcal{P}_2=\tfrac{1}{2}\,\mathrm{Ri}(\mathcal{P}_1-\mathcal{P}_2) \end{aligned}\right\} \quad \text{at} \quad \eta=1, \tag{4.10}$$

$$\left.\begin{aligned} &\frac{d\mathcal{P}_2}{d\eta}-\mathrm{RiRo}\mathcal{P}_2=0 \\ &\frac{d\mathcal{P}_1}{d\eta}-\frac{\mathrm{Ri}}{\tau-1}\mathcal{P}_1=\tfrac{1}{2}\,\mathrm{Ri}(\mathcal{P}_1-\mathcal{P}_2) \end{aligned}\right\} \quad \text{at} \quad \eta=-1. \tag{4.11}$$

Therefore, the mathematical problem which remains is to find those values of τ for a given Ro and Ri which satisfy (4.8)–(4.9) subject to the boundary conditions (4.10)–(4.11). Before investigating the general problem, however, we will examine two special limiting cases: 1) the pure shear waves which occur when $\mathrm{Ri}=0$ and 2) the case of small k.

5. Shear waves

When $\rho_1=\rho_2$ the front becomes vertical. The waves now produce a wave-like displacement in y on this vertical interface, i.e.,

$$\Delta(x,t)=\mathrm{Re}\left\{D\exp\left[ix+i\tau t-\frac{i}{2}\left(\frac{U_1+U_2}{\bar{U}}\right)t\right]\right\}, \tag{5.1}$$

where D is a complex constant. Since in both fluids the horizontal velocity must be nondivergent,

$$i\mathcal{U}_i+\frac{d\mathcal{V}_i}{dy}=0,$$

the pressure perturbations are found to be given by

$$\frac{d^2\mathcal{P}_1}{dy^2}-\mathcal{P}_1=0, \quad \text{for} \quad y\geqslant 0, \tag{5.2}$$

$$\frac{d^2\mathcal{P}_2}{dy^2}-\mathcal{P}_2=0, \quad \text{for} \quad y\leqslant 0, \tag{5.3}$$

if $y=ky^*$.

Requiring the solutions to be finite at $y=\pm\infty$, the solutions to (5.1)–(5.3) may be written

$$\mathcal{P}_1(y\geqslant 0)=A\exp(-y), \tag{5.4}$$

$$\mathcal{P}_2(y\leqslant 0)=B\exp(+y). \tag{5.5}$$

The dynamic boundary condition (i.e., continuity of pressures across the interface) is

$$\mathcal{P}_1-\mathcal{P}_2|_{y=0}=D\left(\frac{d\bar{p}_2}{dy}-\frac{d\bar{p}_1}{dy}\right) \tag{5.6}$$

or

$$A-B=-2D. \tag{5.7}$$

The kinematic conditions are

$$\mathcal{V}_1(y=0)=i(\tau-1)D, \tag{5.8}$$

$$\mathcal{V}_2(y=0)=i(\tau+1)D. \tag{5.9}$$

We may eliminate $\mathcal{V}_1(y=0)$ and $\mathcal{V}_2(y=0)$ by using the semigeostrophic equations (4.6)–(4.7):

$$\mathcal{V}_1(y=0)=i\{1+\mathrm{Ro}(\tau-1)\}A=i(\tau-1)D, \tag{5.10}$$

$$\mathcal{V}_2(y=0)=i\{1-\mathrm{Ro}(\tau+1)\}B=i(\tau+1)D. \tag{5.11}$$

Consequently, (5.7), (5.10) and (5.11) provide three simultaneous homogeneous equations for the three constants D, A and B. Requiring that the determinant vanishes, we find

$$\tau^2=(\mathrm{Ro}-1)/(\mathrm{Ro}+1). \tag{5.12}$$

The results obtained from this simple problem are indicative of the results for the more complex problem when the Richardson number is nonzero. The first significant difference between our results and Orlanski's is that we have lost the stable inertia waves. This is not surprising due to our use of the semigeostrophic equations which filter out high-frequency phenomena (Fjortøft, 1962). However, it does foretell the result that we will miss many of the neutral wave solutions found by Orlanski.

Eq. (5.12) corresponds to the unstable solutions found by Orlanski due to shearing instability. Only when $\mathrm{Ro}\ll 1$ do our solutions correspond closely with Orlanski's. As the Rossby number increases, $|\tau_i|$ decreases monotonically from $|\tau_i|=1$ and eventually becomes zero. This is in marked contrast with Orlanski's results that $|\tau_i|=1$ for all Ro. As we shall see, the $|\tau_i|$ found using the semigeostrophic equations will consistently be smaller than that found using the primitive equations.

For $\mathrm{Ro}\geqslant 1$ the unstable solutions become neutrally stable. Clearly the use of the semigeostrophic equations for these large Rossby numbers is completely unjustified. This phenomenon of the unstable solutions becoming stable at a critical Rossby number was found at all Richardson numbers. Consequently, the use of semigeostrophic equations in the study of instabilities along a Margules front results in a short wavelength cutoff.

6. Instability of very long waves

In this section we examine the behavior of the general problem (4.8)–(4.9) for small Ro. This will be done by formally taking the limit of the $\mathrm{Ro}\to 0$ in (4.8)–(4.9) which yields

$$\frac{d}{d\eta}\left[(1+\eta)\frac{d\mathcal{P}_1}{d\eta}\right]-\frac{\mathrm{Ri}}{\tau-1}\mathcal{P}_1=\tfrac{1}{2}\,\mathrm{Ri}(\mathcal{P}_1-\mathcal{P}_2), \tag{6.1}$$

$$\frac{d}{d\eta}\left[(\eta-1)\frac{d\mathcal{P}_2}{d\eta}\right]-\frac{\mathrm{Ri}}{\tau+1}\mathcal{P}_2=\tfrac{1}{2}\,\mathrm{Ri}(\mathcal{P}_1-\mathcal{P}_2), \tag{6.2}$$

with

$$\frac{d\mathcal{P}_1}{d\eta}=0 \quad \text{at} \quad \eta=1, \quad \frac{d\mathcal{P}_2}{d\eta}=0 \quad \text{at} \quad \eta=-1. \tag{6.3}$$

Eqs. (6.1)–(6.3) are identical to Orlanski's (5.6)–(5.8).

Orlanski showed that the eigenvalue problem may be reduced to solving the ordinary differential equation

$$(1-\eta^2)\frac{d^2\phi}{d\eta^2}+(r+s\eta)\phi=0, \quad \phi(\pm 1)=0, \tag{6.4}$$

where the constants r and s are

$$r=\mathrm{Ri}\left(\frac{1+\tau^2}{1-\tau^2}\right) \quad \text{and} \quad s=\mathrm{Ri}\left(\frac{-2\tau}{1-\tau^2}\right).$$

Eq. (6.4) was shown to have solutions for $\tau=0$ only if $\mathrm{Ri}=n(n+1)$, where $n=1, 2, \ldots$; otherwise $\tau=0$ is not a solution when $\mathrm{Ro}=0$.

For nonzero τ, Orlanski was forced to solve the eigenvalue problem using a numerical variational method. Instead of using Orlanski's method to solve (6.4), we shall solve it as follows: If τ is nonzero, we may introduce a new dependent variable ψ such that

$$\psi=\tau\phi. \tag{6.5}$$

Using ψ, Eq. (6.4) may be rewritten

$$[(1-\eta^2)\phi_{\eta\eta}+\mathrm{Ri}\phi] -\tau[(1-\eta^2)\psi_{\eta\eta}-\mathrm{Ri}\psi-2\eta\,\mathrm{Ri}\psi]=0, \tag{6.6a}$$

with

$$\left.\begin{aligned}\psi-\tau\phi&=0\\ \phi(1)=\phi(-1)=\psi(1)=\psi(-1)&=0\end{aligned}\right\}. \tag{6.6b}$$

Upon finite differencing (6.6a), Eq. (6.6) reduces to the

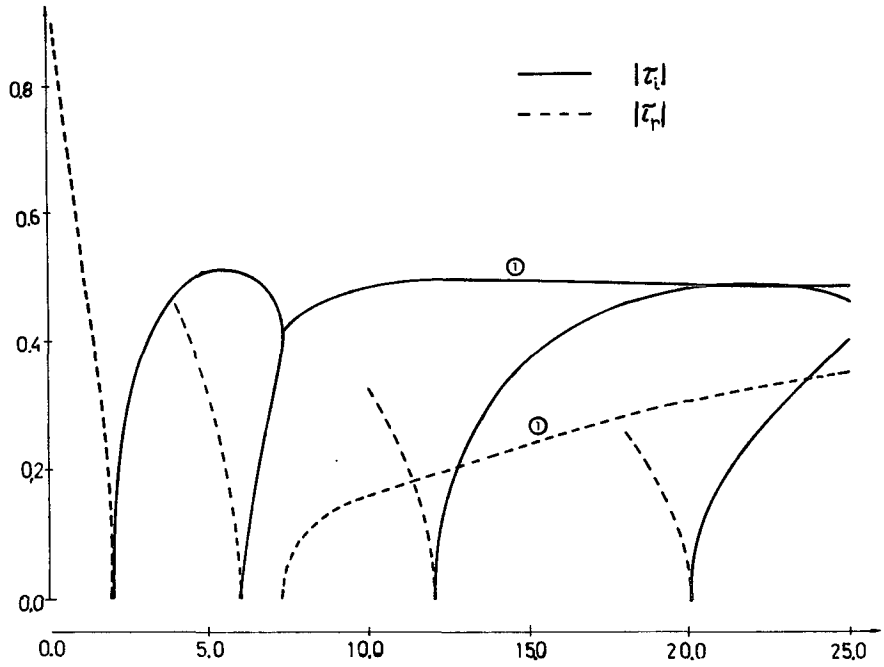

FIG. 2. The complex phase speed τ as a function of Richardson number for Ro=0. We have displayed only the $|\tau_r|$ of an internal wave just before it develops a nonzero τ_i.

standard form

$$(A-\tau B)\mathbf{x}=\mathbf{0}, \tag{6.7}$$

where A and B are the matrices holding the coefficients from the set of linear equations resulting from the finite differencing and $\mathbf{x}$ the eigenvector $(\psi_1,\phi_1,\psi_2,\phi_2,\ldots,\psi_N,\phi_N)$. Since the matrix B is pentadiagonal, it may be rapidly inverted. A is then multiplied by B^{-1} so that

$$(B^{-1}A-\tau I)\mathbf{x}=\mathbf{0}. \tag{6.8}$$

The eigenvalues were found using numerical methods explained in Appendix B.

Finite differencing the interval $(-1, 1)$ so that there are 40 grid points, Fig. 2 shows some of the eigenvalues found as a function of Ri. For very small Ri, 40 pairs of neutrally stable waves with $\tau_r\approx\pm1$ are found; they correspond to internal waves. (The number of waves which can be resolved depends upon the resolution of the finite-differencing in the y direction.) As Ri increases, the phase speed of these waves becomes smaller; in particular, the phase speed of a particular pair (shown in Fig. 2) drops extremely rapidly so that it becomes zero at Ri=2. For Ri>2, this pair developed a purely imaginary phase speed so that these disturbances will grow, at least initially, exponentially with time.

Similarly, at Ri=6, 12, ..., the phase speed of a pair of internal waves becomes zero, followed by the generation of another unstable mode. (We have chosen to display the pair of internal waves just before they develop a zero phase speed to simplify the figure.) As can be seen from Fig. 2, after the critical Richardson number the complex phase speed may eventually develop a nonzero real *and* imaginary part.

Upon comparing our results with Orlanski's, we find that the agreement is excellent. As Orlanski has already demonstrated, the physical interpretation of these unstable modes is the presence of quasigeostrophic baroclinic instability for Ri>2 at small Rossby number.

7. The general case

In this section the solutions to the general problem are presented as formulated with the semigeostrophic equations; these solutions were obtained by the numerical integrations of (4.8)–(4.11). Unlike Orlanski's problem, Appendix A shows that the finite-differenced form of (4.8)–(4.11) may be so manipulated that the resulting set of algebraic equations results in a linear eigenvalue problem. The numerical techniques used to find the eigenvalues and eigenvectors in this paper are discussed in Appendix B.

I have explored the solution to the system (4.8)–(4.11) for the general range $0\leqslant$Ri$\leqslant25$ and $0\leqslant$Ro$\leqslant1$ with the primary emphasis on non-real values of τ. Whenever possible I have compared my results with Orlanski's results by placing his computed values of τ_r and τ_i (as found in his Appendix C) on the figures of this paper as "data points."

In Section 5 it was demonstrated that if Ri=0 there would be a nonzero τ_i (with $\tau_r=0$) if Ro<1. As Ro increased from zero to one, $|\tau_i|$ decreased monotonically from its maximum value of one to zero. The physical interpretation of this unstable solution is

readily shown to be the well-known phenomenon of shearing instability in homogeneous, incompressible fluids of the same density, i.e., Rayleigh instability.

For $0<\mathrm{Ri}\leqslant 2$, it is also found that $|\tau_i|$ decreases monotonically from its maximum value of one at $\mathrm{Ro}=0$ to zero as the Rossby number increases. As Figs. 3 and 4 show, however, the Rossby number at which $|\tau_i|$ becomes zero has been reduced from one to some smaller value.

When $\mathrm{Ri}>2$, the stability properties of the flow become more complex. For $\mathrm{Ri}=2.03$ (Fig. 5), in addition to a stability curve similar to that which occurs for $\mathrm{Ri}\leqslant 2$, a new stability curve appears. This is the continuation into the region of nonzero Ro of the unstable solution resulting from quasigeostrophic baroclinic instability found in Section 6 when $\mathrm{Ri}>2$.

The stability diagrams associated with $\mathrm{Ri}=2.41$ and $\mathrm{Ri}=2.5$ (Figs. 6 and 7) are radical departures from the stability diagrams found for smaller Ri; the stability diagram shown in Fig. 6 behaves, for example, in such a manner that three distinct "regions" may be discerned. The first region has two different τ_i and a zero τ_r; one of them is the extension into the region of nonzero Ro of the unstable solution found in Section 6 for $\mathrm{Ri}>2$, and the other is a modified form of the

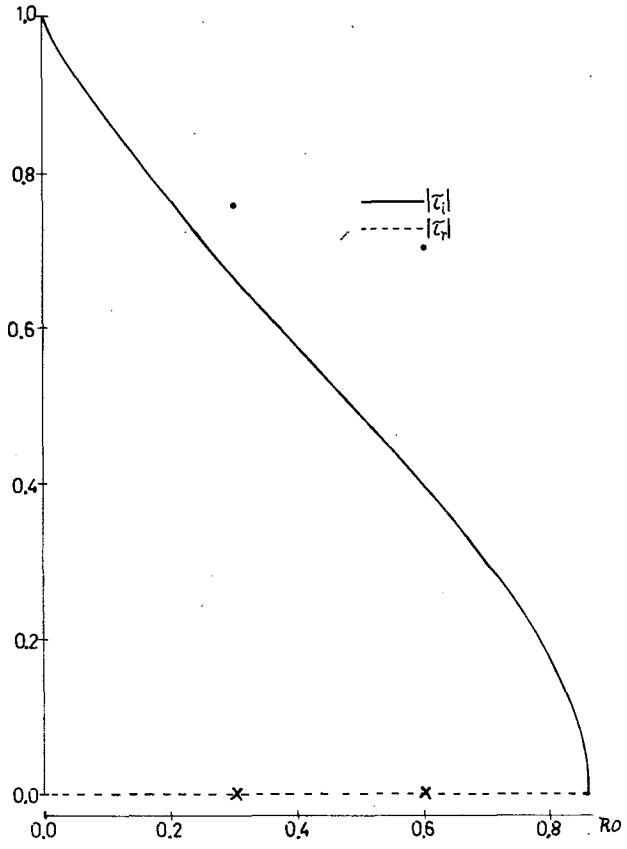

FIG. 3. The complex phase speed τ as a function of Ro at Ri $=1.00$. The data points (×, ●) denote the $|\tau_r|$ and $|\tau_i|$ found by Orlanski (1968), respectively.

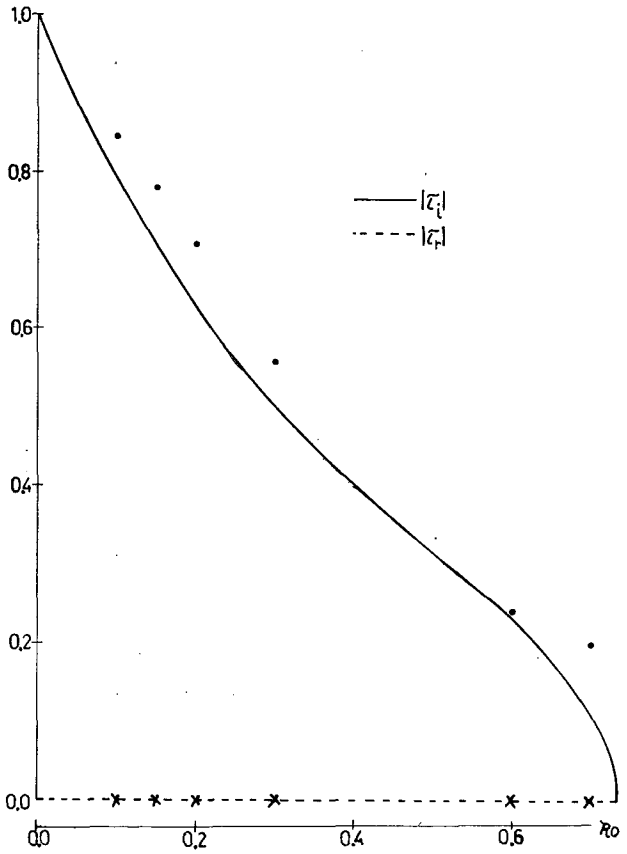

FIG. 4. As in Fig. 3 except at $\mathrm{Ri}=2.00$.

stability curve found when $\mathrm{Ri}\leqslant 2$. As Ro increases these two curves eventually coalesce and, in region 2 become the complex conjugates of each other. At even larger Ro a third region appears where the curves again separate and τ_r is zero. For sufficiently high Ro the flow becomes stable.

Fig. 8 shows the stability of the flow for $\mathrm{Ri}=3$. It has properties similar to Figs. 6 and 7 with the exception that region 3 is separated from region 2 by an area of neutral stability. As Ri becomes larger, this third region of instability eventually disappears (Figs. 9 and 10).

Another phenomenon which Figs. 8 and 9 show is that the Rossby number at which region 1 ends becomes smaller and smaller as Ri increases. Eventually, for this *particular* stability curve region 1 will disappear completely (see Fig. 11, Curve 2).

In Figs. 11 and 12 we show the stability diagrams for $\mathrm{Ri}=10$ and 25. The behavior of the stability curves is similar to the behavior of the stability curves found for smaller Ri.

From the results presented in this section, as well as Section 5, we see that the $|\tau_i|$ found by using the semigeostrophic equations consistently underestimates the $|\tau_i|$ found by using the primitive equations except when $\mathrm{Ro}=0$. It is readily shown that the semigeostrophic equations assume that $(\mathrm{Ro}^2/v)(D^2v/Dt^2)$ and $(\mathrm{Ro}^2/u)(D^2u/Dt^2)$ are much less than 1. Fjortøft

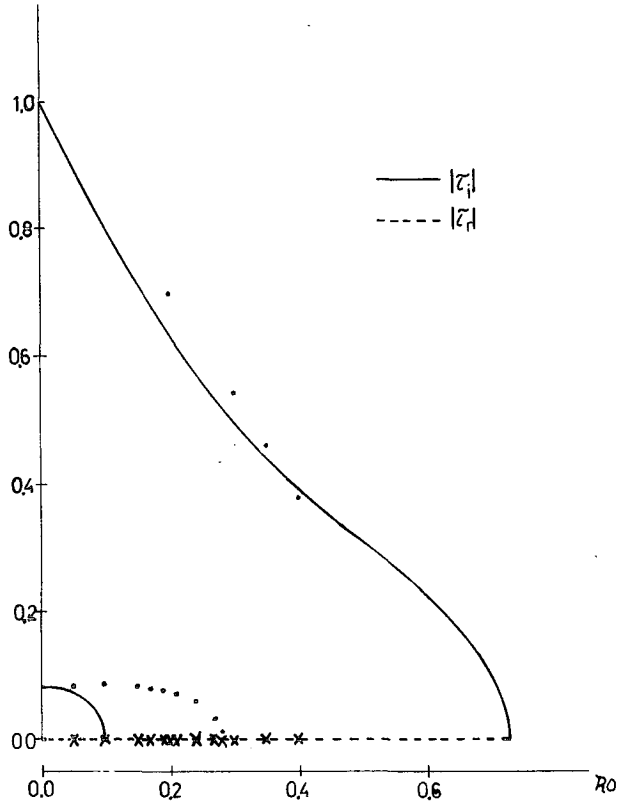

FIG. 5. As in Fig. 3 except at Ri=2.03.

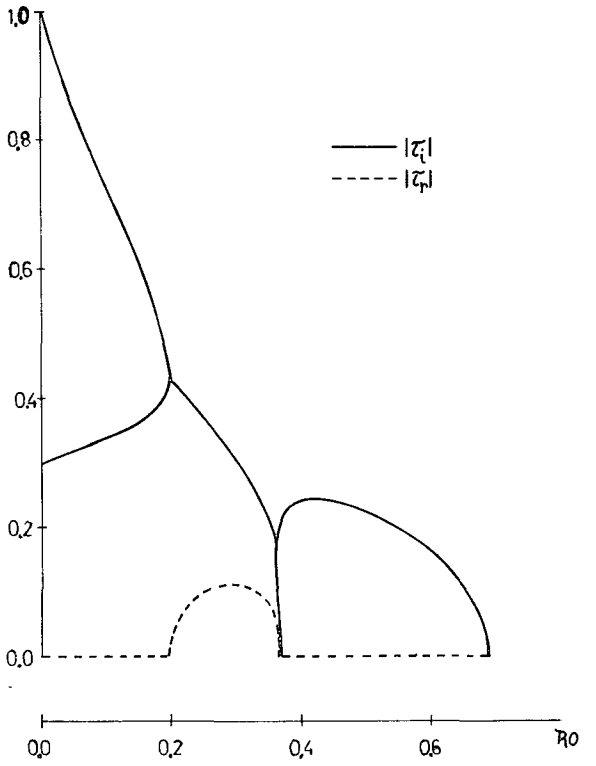

FIG. 7. As in Fig. 3 except at Ri=2.50.

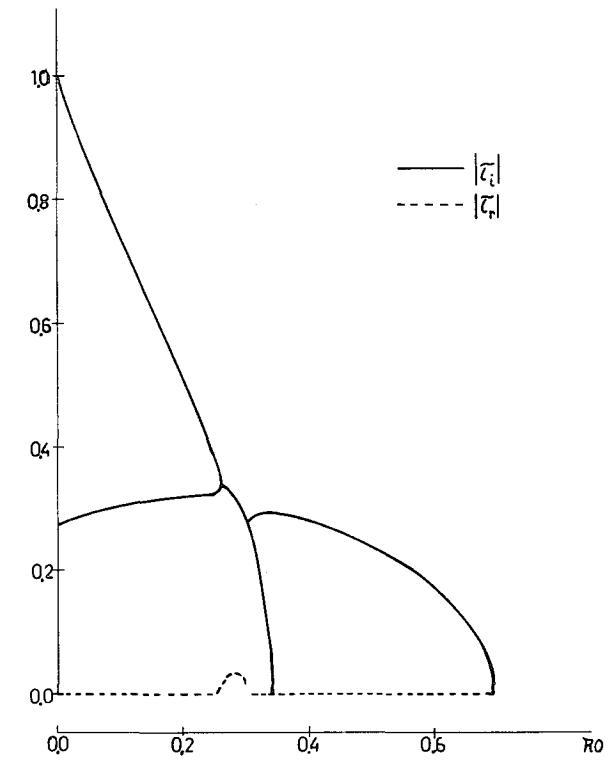

FIG. 6. As in Fig. 3 except at Ri=2.41.

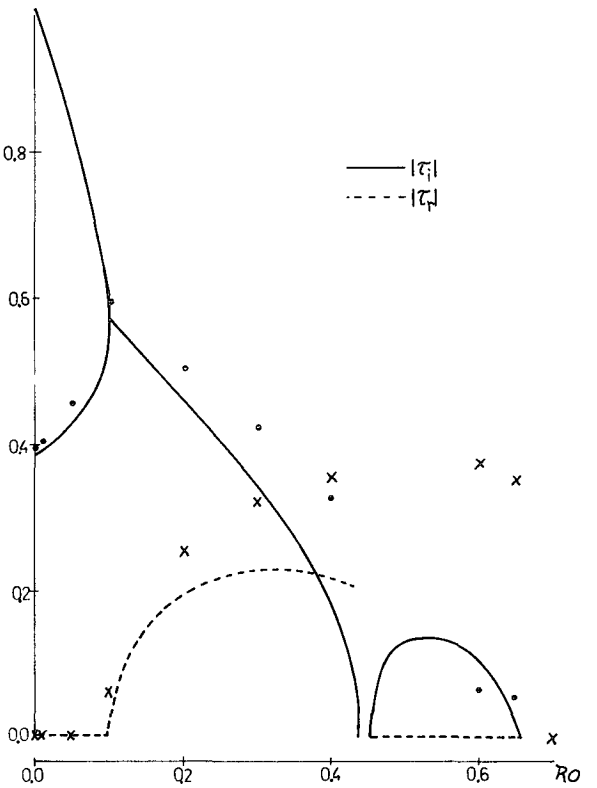

FIG. 8. As in Fig. 3 except at Ri=3.00.

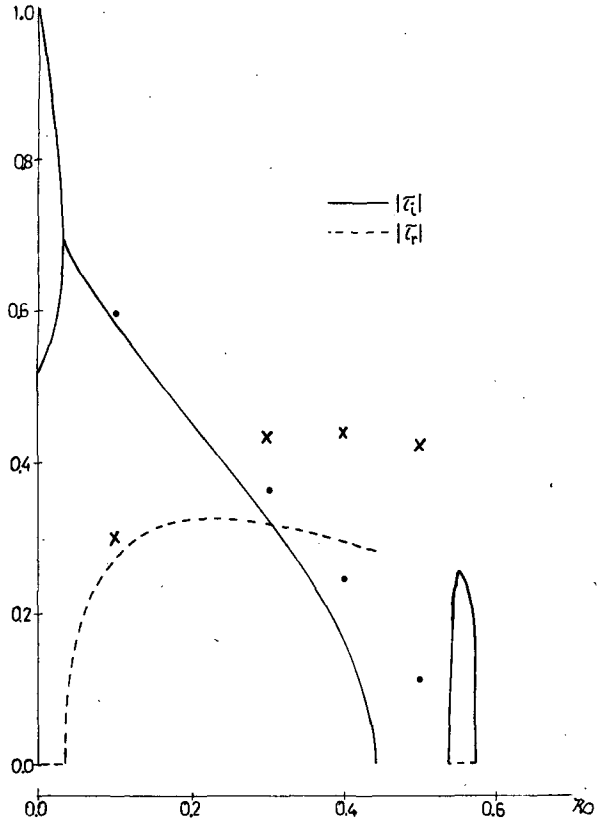

FIG. 9. As in Fig. 3 except at Ri=5.00.

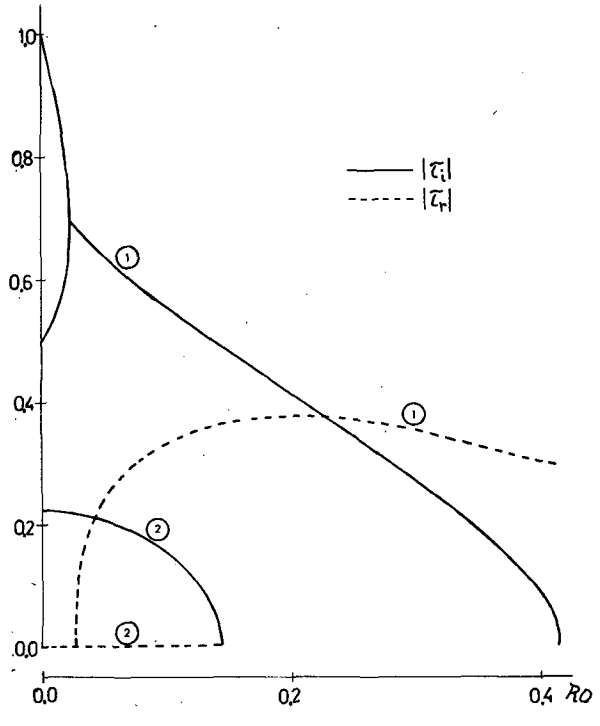

FIG. 10. As in Fig. 3 except at Ri=6.50.

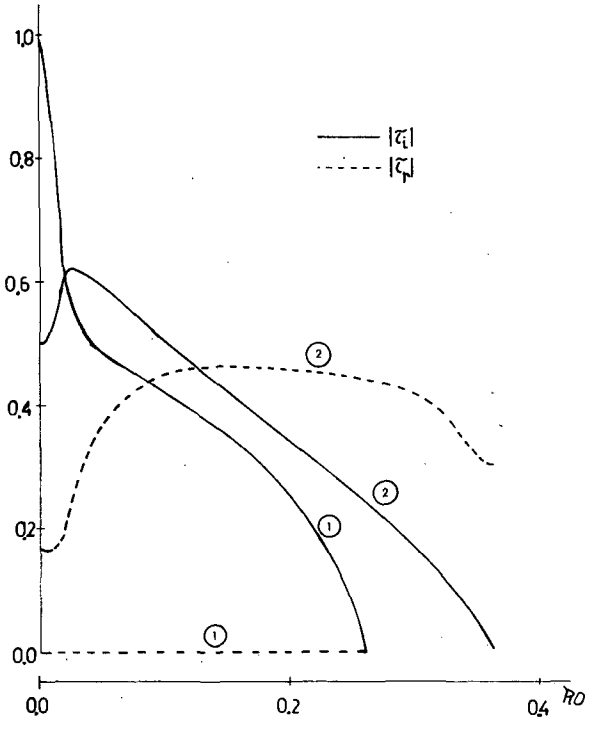

FIG. 11. As in Fig. 3 except at Ri=10.00.

(1962) has interpreted this condition to imply that the semigeostrophic equations neglect high-frequency phenomena. If unstable solutions exist in the flow field, another interpretation of this condition is that the unstable perturbations may not grow too rapidly. Consequently it is not surprising that the semigeostrophic equations should produce unstable perturbation solutions which grow less rapidly than those found using the primitive equations.

To make our study absolutely complete, we could recalculate the solutions using the quasigeostrophic equations to see how much more insight one can gain with the semigeostrophic equations. However, if we make the substitution $s=\mathrm{Ri}^{\frac{1}{2}}\eta$ in (4.8)–(4.9), we find that the perturbation equations derived from the semigeostrophic and quasigeostrophic equations are identical to each other in the limit of large Richardson number. Consequently the semigeostrophic equations are able to capture those physical phenomena which occur when the Richardson number is not large and which would be missed by the quasigeostrophic equations.

From the values plotted from Orlanski's paper, we see that the agreement between our results and his results was good if $\mathrm{Ro}\leqslant 0.4$. There were also cases where there was good agreement between Orlanski's and our results when $\mathrm{Ro}\geqslant 0.4$; however, there did not appear to be any consistent patterns to these cases.

Finally, if λ denotes the Rossby radius of deformation, then

$$k/(1/\lambda)=\mathrm{Ro}f\bar{U}^{-1}(NH/f),$$

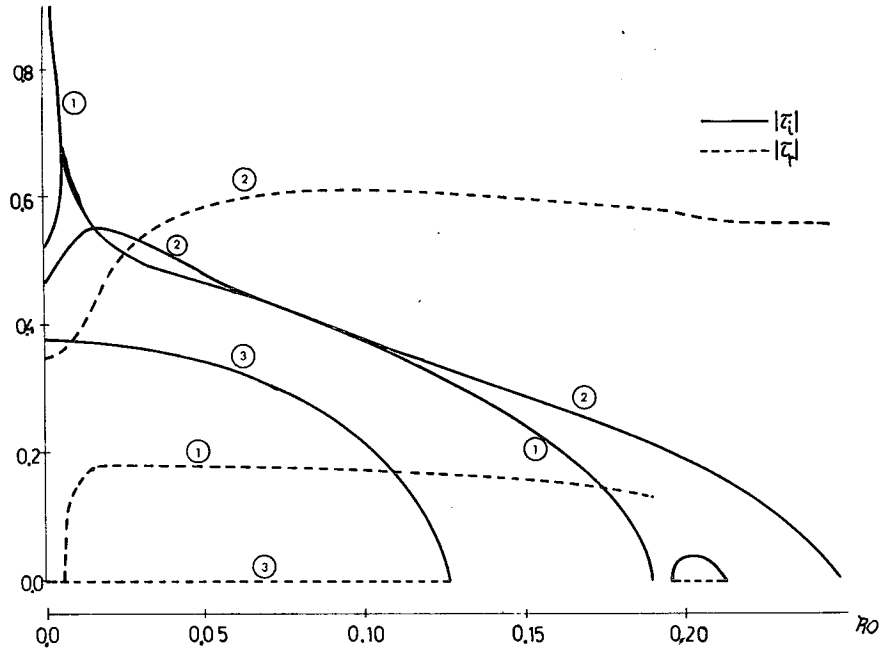

FIG. 12. As in Fig. 3 except Ri=25.00.

where N is the Brunt–Väisälä frequency. In our model

$$N=(4g\Delta\rho/\bar{\rho}H)^{\frac{1}{2}},$$

where $\Delta\rho=\rho_1-\rho_2$. Consequently,

$$k/(1/\lambda)=\mathrm{Ro}(4g\Delta\rho/\bar{\rho}H)^{\frac{1}{2}}H\bar{U}^{-1}=4\ \mathrm{RoRi}^{\frac{1}{2}}. \quad (7.1)$$

For a given Ri, I have computed the right-hand side of (7.1) for the Ro which gave the largest growth rate; the results are presented in Table 1. From Table 1 we see that the most unstable perturbation, which will eventually overshadow all the other perturbations, has a characteristic length scale of approximately one-third to one-half of the Rossby radius of deformation.

8. Kinematics of a frontal wave

In this section I describe the velocity and height fields associated with an unstable perturbation found in Section 7. I have chosen the unstable solution $\tau=0.27376-i0.58353$, when Ri=5 and Ro=10^{-1}; it is our counterpart to the wave chosen by Orlanski to study the kinematics of a meteorological frontal wave.

Fig. 13 shows h' over one wavelength in the zonal direction and over $0\leqslant y\leqslant 2$. Figs. 14–19 show w_1', w_2', u_1', u_2', v_1' and v_2' of the unstable wave. Except for w_1' and

TABLE 1. The ratio of Rossby radius of deformation to the length scale of the most unstable perturbation for a given Richardson number.

Richardson number	Rossby number of most unstable perturbation	$k\lambda$
1.00	0.525	2.10
2.00	0.450	2.55
2.03	0.430	2.45
2.41	0.450	2.80
2.50	0.400	2.53
3.00	0.300	2.08
5.00	0.280	2.50
6.50	0.230	2.35
10.00	0.200	2.53
25.00	0.150	3.00

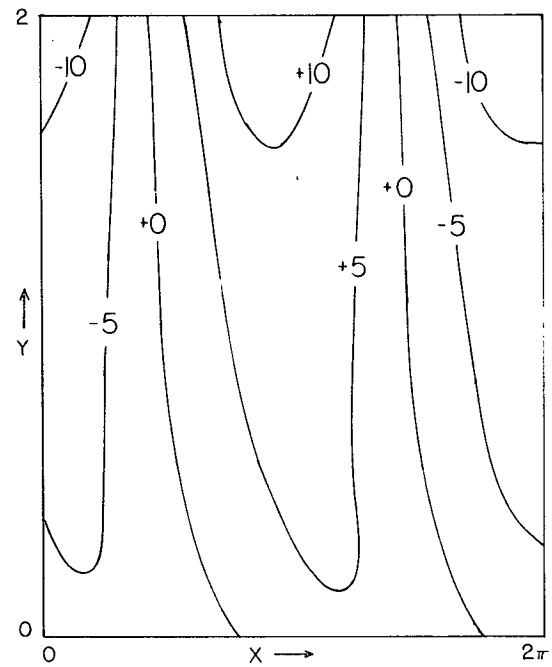

FIG. 13. The perturbation height field h' in the frontal zone. Units are nondimensional.

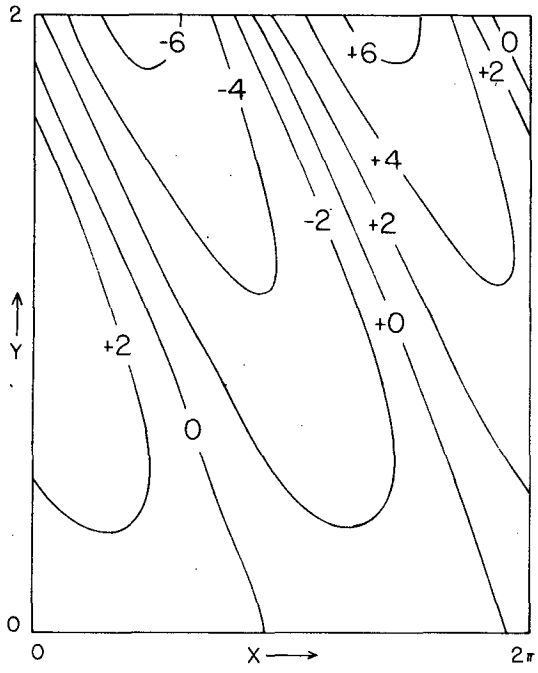

FIG. 14. The perturbation vertical velocity w_1' in the frontal zone. Units are nondimensional.

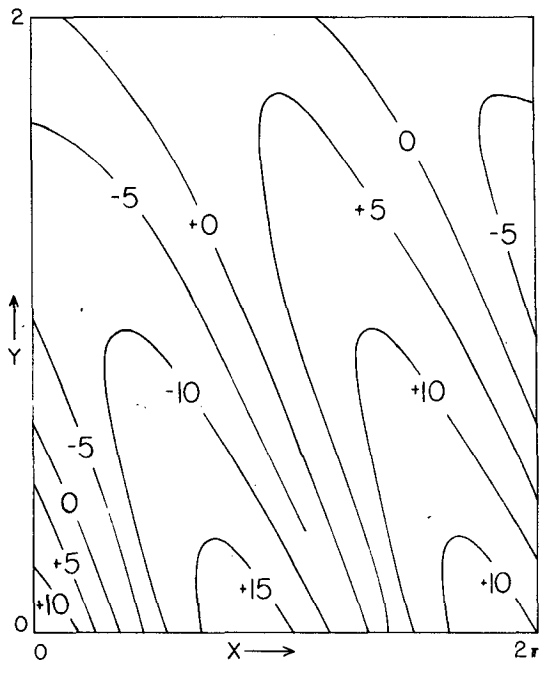

FIG. 16. The perturbation zonal velocity u_1' in the frontal zone. Units are nondimensional.

w_2' the maximum perturbation amplitude is largest in layer 2.

9. Energetics

In the study of complex hydrodynamic instabilities an examination of the energy transformations is frequantly useful. Large-scale atmospheric instabilities are often classified as either being baroclinic or barotropic depending upon whether the perturbations draw their energy from the available potential energy or the kinetic energy of the basic state. In this section we shall examine the energy transformations associated with the unstable solutions found in Section 7.

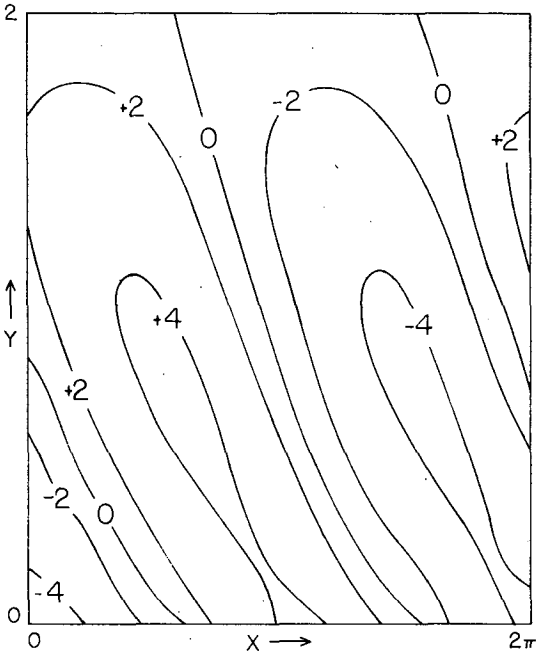

FIG. 15. As in Fig. 14 except for w_2'.

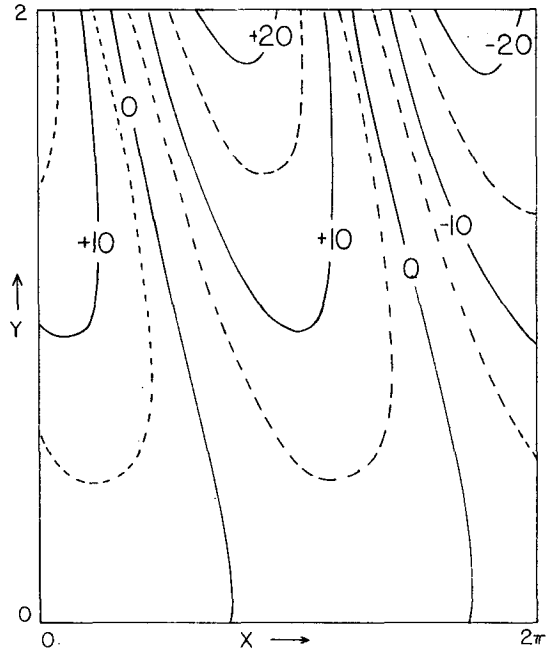

FIG. 17. As in Fig. 16 except for u_2'.

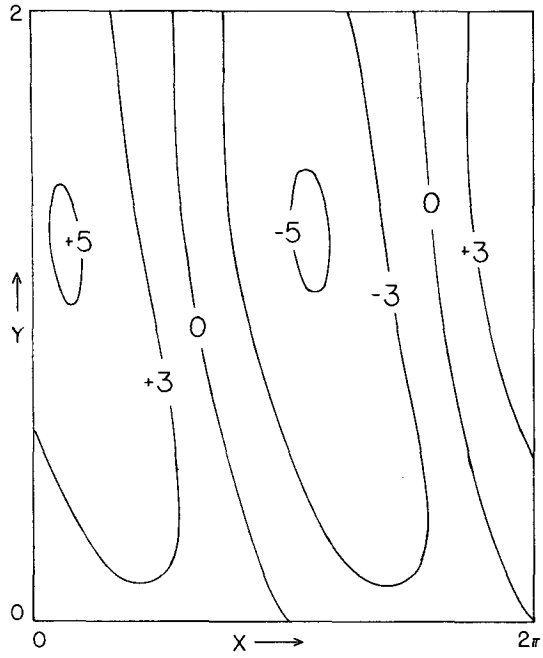

FIG. 18. The perturbation meridional velocity v_1' in the frontal zone. Units are nondimensional.

If we rewrite the continuity equation as

$$(\phi_1'-\phi_2')_t=w_1'-\frac{1}{\mathrm{RiRo}}\frac{d\bar{h}}{dy}v_1'-\frac{U_1}{\bar{U}}(\phi_1'-\phi_2')_x, \quad (9.1)$$

$$(\phi_1'-\phi_2')_t=w_2'-\frac{1}{\mathrm{RiRo}}\frac{d\bar{h}}{dy}v_2'-\frac{U_2}{\bar{U}}(\phi_1'-\phi_2')_x, \quad (9.2)$$

we may form a potential energy equation by multiplying (9.1) by $U_1(\phi_1'-\phi_2')/2\bar{U}$ and (9.2) by $U_2(\phi_1'-\phi_2')/2\bar{U}$. If $\int(\ )da$ denotes the areal integral over one wavelength and over the interval $[-\infty, \infty]$ in the y direction, then the change of the eddy available potential energy (APE) is given by

$$\underbrace{\frac{d}{dt}\int\tfrac{1}{2}(\phi_1'-\phi_2')^2da}_{①}$$

$$=\underbrace{\int\left(\frac{U_1}{2\bar{U}}v_1'h'-\frac{U_2}{2\bar{U}}v_2'h'\right)\left(\frac{1}{\mathrm{RiRo}}\frac{d\bar{h}}{dy}\right)da}_{④}$$

$$\underbrace{-\int\left(\frac{U_1}{2\bar{U}}w_1'h'-\frac{U_2}{2\bar{U}}w_2'h'\right)da}_{⑤}. \quad (9.3)$$

As Orlanski (1968) has shown, integral ④ represents the increase of the eddy APE at the expense of the basic state's APE through the northward transport of negative h' particles and the southward transport of positive h' particles. Noting the strong analog between $-h$ of our problem and the form of the potential temperature (thickness) found in two-level models, we may further interpret integral ④ as representing the southward transport of "cold air" and the northward transport of "warm air"—a process characteristic of quasigeostrophic baroclinic instability discovered by Charney (1947) and Eady (1949).

Orlanski (1968) has shown that integral ⑤ represents the transformation of the eddy APE into the eddy kinetic energy (KE) by a positive correlation in x of descending motion with positive h'. If we again make the analog between our h and the form of the potential temperature as formulated in two-level models, we may further interpret integral ⑤ as the transformation of the eddy APE into the eddy KE by the rising of "warm air" and the sinking of "cold air."

It is interesting to note that although the eigenvalue τ depends only upon the values of the Rossby and Richardson numbers, the energetics depends not only upon Ri and Ro but also the nondimensional velocities of each of the layers, $U_1/\bar{U}$ and $U_2/\bar{U}$.

Turning to the momentum equations, we find that the perturbations are governed by

$$\frac{\mathrm{Ro}}{\mathrm{RoRi}}\left(\frac{\partial}{\partial t}+\frac{U_2}{\bar{U}}\frac{\partial}{\partial x}\right)\frac{\partial\phi_2'}{\partial y}+v_2'=\frac{\partial\phi_2'}{\partial x}, \quad (9.4)$$

$$\mathrm{Ro}\left(\frac{\partial}{\partial t}+\frac{U_2}{\bar{U}}\frac{\partial}{\partial x}\right)\frac{\partial\phi_2'}{\partial x}+u_2'=-\frac{1}{\mathrm{RiRo}}\frac{\partial\phi_2'}{\partial y}, \quad (9.5)$$

$$\frac{\mathrm{Ro}}{\mathrm{RoRi}}\left(\frac{\partial}{\partial t}+\frac{U_1}{\bar{U}}\frac{\partial}{\partial x}\right)\frac{\partial\phi_1'}{\partial y}+v_1'=\frac{\partial\phi_1'}{\partial x}, \quad (9.6)$$

$$\mathrm{Ro}\left(\frac{\partial}{\partial t}+\frac{U_1}{\bar{U}}\frac{\partial}{\partial x}\right)\frac{\partial\phi_1'}{\partial x}+u_1'=-\frac{1}{\mathrm{RiRo}}\frac{\partial\phi_1'}{\partial y}. \quad (9.7)$$

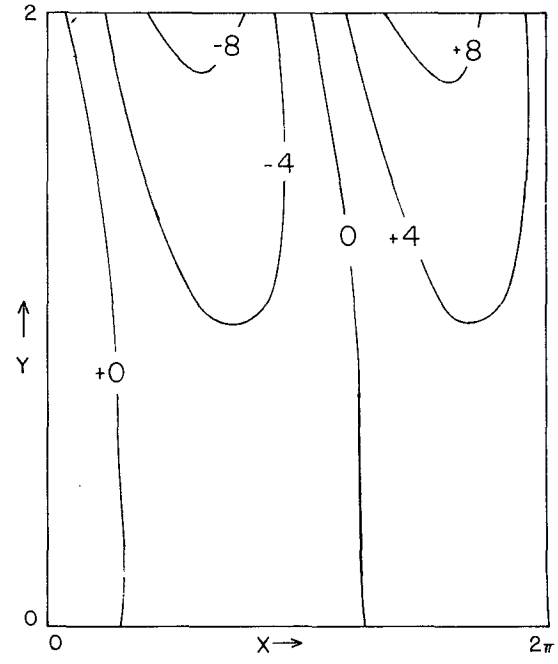

FIG. 19. As in Fig. 18 except for v_2'.

After multiplying (9.4) by $(4\,\mathrm{RiRo}-\bar{h})\partial\phi_2'/\mathrm{RoRi}\partial y$, (9.5) by $(4\,\mathrm{RiRo}-\bar{h})\partial\phi_2'/\partial x$, (9.6) by $\bar{h}\partial\phi_1'/\mathrm{RoRi}\partial y$ and (9.7) by $\bar{h}\partial\phi_1'/\partial x$, we have

$$\underbrace{\frac{d}{dt}\int\frac{\mathrm{Ro}}{(\mathrm{RoRi})^2}\left[(4\,\mathrm{RiRo}-\bar{h})\frac{1}{2}\frac{\partial\phi_2'^2}{\partial y}+\bar{h}\frac{1}{2}\frac{\partial\phi_1'^2}{\partial y}\right]+\mathrm{Ro}\left[(4\,\mathrm{RiRo}-\bar{h})\frac{1}{2}\frac{\partial\phi_2'^2}{\partial x}+\bar{h}\frac{1}{2}\frac{\partial\phi_1'^2}{\partial x}\right]da}_{②}$$

$$=\int\frac{1}{\mathrm{RiRo}}\left[(4\,\mathrm{RiRo}-\bar{h})\frac{\partial\phi_2'}{\partial y}v_2'+\bar{h}\frac{\partial\phi_1'}{dy}v_1'\right]+\left[(4\,\mathrm{RiRo}-\bar{h})u_2'\frac{\partial\phi_2'}{\partial x}+\bar{h}u_1'\frac{\partial\phi_1'}{\partial x}\right]da. \quad (9.8)$$

Integral ② represents the rate of change of the KE of the perturbations due to the source term on the right-hand side of (9.8). This source term, however, does not have any clear physical interpretation. For that reason we employ the continuity equation in conjunction with x-momentum equations to rewrite (9.8) as

$$\underbrace{\frac{d}{dt}\int\frac{\mathrm{Ro}}{(\mathrm{RoRi})^2}\left\{(4\,\mathrm{RiRo}-\bar{h})\frac{1}{2}\left(\frac{\partial\phi_2'}{\partial y}\right)^2+\bar{h}\frac{1}{2}\left(\frac{\partial\phi_2'}{\partial y}\right)^2\right\}+\mathrm{Ro}\left[(4\,\mathrm{RiRo}-\bar{h})\frac{1}{2}\left(\frac{\partial\phi_2'}{\partial x}\right)^2+\bar{h}\frac{1}{2}\left(\frac{\partial\phi_1'}{\partial x}\right)^2\right]da}_{②}$$

$$+\underbrace{\frac{d}{dt}\int\frac{1}{\mathrm{Ri}}\left(\frac{U_2}{\bar{U}}h'\frac{\partial\phi_2'}{\partial y}-\frac{U_1}{\bar{U}}h'\frac{\partial\phi_1'}{\partial y}\right)da}_{③}$$

$$=\underbrace{\int\frac{1}{\mathrm{Ri}}\left(\frac{U_2}{\bar{U}}w_2'\frac{\partial\phi_2'}{\partial y}-\frac{U_1}{\bar{U}}w_1'\frac{\partial\phi_1'}{\partial y}\right)da}_{⑥}-\underbrace{\int\frac{1}{\mathrm{Ri}}\left(\frac{1}{\mathrm{RiRo}}\frac{d\bar{h}}{dy}\right)\left(\frac{U_2}{\bar{U}}v_2'\frac{\partial\phi_2}{\partial y}-v_1'\frac{\partial\phi_1'}{\partial y}\right)da}_{⑦}+\underbrace{\int\frac{U_1}{2\bar{U}}w_1'h'-\frac{U_2}{2\bar{U}}w_2'h'da}_{⑧}. \quad (9.9)$$

In addition to the integral ② which represents the rate of change of the perturbation's KE, we find an integral ③ in this reformulation of (7.8) whose physical interpretation is as follows:

Since the actual flow consists of small perturbations superimposed upon a mean flow, the actual interface between fluid 1 and fluid 2 is not $\bar{h}$ but rather an interface which undulates about $\bar{h}$. This oscillation of the interface results in intrusions of fluid 1 into regions where there had been only fluid 2 and vice versa. Since an intrusion will usually have momentum different from that of the fluid that it is displacing, the eddy kinetic energy of the flow will consist of two sources: the kinetic energy of the disturbances and the kinetic energy arising from this exchange process which Orlanski has called the "interaction kinetic energy."

As (9.9) shows, the rate of change of the eddy KE given by the sum of integrals ② and ③ results from three physical processes. As has already shown, integral ⑤ represents the increase of eddy KE at the expense of eddy APE. Integrals ⑥ and ⑦ represent sources of eddy KE due to Rayleigh and Kelvin–Helmholtz instability, respectively.

I have computed numerically the integrals ①, ②+③, ⑤ and ⑥+⑦ for various Ri and Ro; the results are presented in Table 2. I have normalized the results so that integral ④ = 1 and have taken $U_2/\bar{U}=1.5$ and $U_1/\bar{U}=-0.5$. For a given Richardson number, those Rossby numbers are examined where there is a maximum in the growth rate. In those cases where there are several stability curves present I examined the maxima present for each stability curve.

As Table 2 shows, for the majority of cases studied the eddy APE increases by the conversion of the basic state's APE into eddy APE. A portion of the eddy APE is then converted into eddy KE. Finally some of the eddy KE is fed back into the basic state to increase its kinetic energy.

An exception to this is the case of Ri = 1. Here both the basic state's APE and KE are tapped to produce the eddy APE and KE.

An interesting discovery is the appearance of certain cases where the eddy KE is decreasing with time although the system is unstable. This results from a large negative integral ③. The physical interpretation is that although the perturbations may act in such a

TABLE 2. Energy conversions created by unstable perturbations for a given Rossby and Richardson number.

Ro	Ri	τ_r	τ_i	①	②+③	⑤	⑥+⑦
0.525	1.000	0.0000	−0.463	0.6925	0.9718	0.3074	0.6644
0.450	2.000	0.0000	−0.355	0.6149	0.2697	0.3851	−0.1154
0.050	2.030	0.0000	−0.071	0.6421	−0.4456	0.3579	−0.8034
0.450	2.030	0.0000	−0.349	0.6109	0.2613	0.3891	−0.1277
0.200	2.410	0.0000	−0.513	0.7969	−0.1311	0.2031	−0.3343
0.500	2.410	0.0000	−0.239	0.5277	0.2864	0.4723	−0.1859
0.250	2.500	0.1015	−0.3693	0.7515	−0.1639	0.2485	−0.4123
0.500	2.500	0.0000	−0.2223	0.5210	0.2668	0.4790	−0.2122
0.300	3.000	0.2280	−0.3450	0.6656	0.1416	0.3344	−0.1929
0.550	3.000	0.0000	−0.1330	0.4598	0.3220	0.5402	−0.2183
0.275	5.000	0.3231	−0.3555	0.5555	0.2905	0.4445	−0.1541
0.555	5.000	0.0000	−0.0260	0.4097	0.1973	0.5903	−0.3931
0.100	6.500	0.3394	−0.5540	0.8276	−0.0211	0.1724	−0.1934
0.240	6.500	0.3723	−0.3540	0.5618	0.2536	0.4382	−0.1846
0.175	10.000	0.0000	−0.3098	0.3313	0.3273	0.6687	0.3416
0.200	10.000	0.4581	−0.3475	0.5681	0.2312	0.4319	−0.2007
0.085	25.000	0.0000	−0.2677	0.2920	0.4336	0.7080	−0.2744
0.120	25.000	0.1675	−0.3279	0.3026	0.4336	0.6974	−0.2639
0.150	25.000	0.5954	−0 2899	0.5639	0.1937	0.4361	−0.2424
0.205	25.000	0.0000	−0.3636	0.2100	0.4256	0.7900	−0.3644

manner as to increase the eddy APE, the intrusions of fluid 1 into regions which had previously contained fluid 2 and vice versa are occurring in such a manner that ⑥+⑦ is negative and much larger in magnitude than ⑤.

10. Conclusion

In this paper we have examined unstable waves on a Margules front using the semigeostrophic equations. In addition to finding the complex phase speeds of the unstable waves as a function of Rossby and Richardson numbers, we also examined the kinematics and energetics of unstable waves.

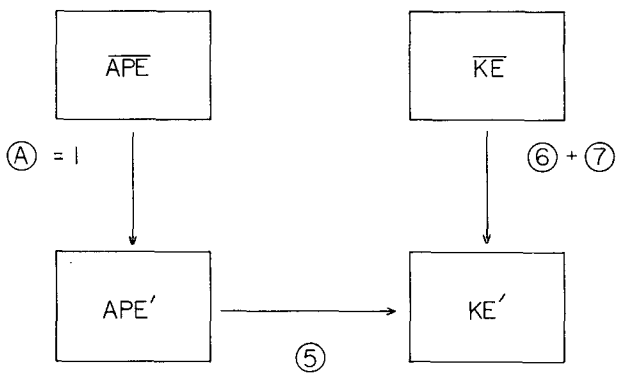

FIG. 20. Energy flow diagram for the frontal instability.

As stated in the introduction, the primary purpose of this paper is to investigate the value of the semigeostrophic equations for obtaining approximate solutions to the primitive equations. This was done by applying the semigeostrophic equations to a meteorological problem which had already been solved through the use of the primitive equations. Based upon the results from the previous sections, it may be concluded that the semigeostrophic equations are an adequate approximation to the primitive equations for $Ro^2 \ll 1$ and Ri is not much less than 1.

In Section 7 we saw that for $Ro \leqslant 0.4$ the semigeostrophic equations captured the essence of the instability although it consistently underestimated the value of $|\tau_i|$. This means that the semigeostrophic equations are able to capture conventional baroclinic instability and large-scale shear instability but will miss small-scale Rayleigh and Kelvin–Helmholtz instabilities.

Finally, although the semigeostrophic equations approximate the primitive equations more closely than the quasigeostrophic equations, the above discussion does not imply that the semigeostrophic formulation is superior to the balance equations.

Acknowledgments. The author wishes to express his thanks to Lt. Col. Thomas W. Flattery and Capt. Harry W. Henderson for their readings of the manuscript and many useful discussions. He also wishes to

thank Sgt. Jeffery L. Hoskin for his careful drawing of the figures.

APPENDIX A

Finite Differencing of the Perturbation Equations

In order to derive the finite-differenced form of the perturbation equations (4.8)–(4.11), we introduce two sets of constants $\phi_1^{(n)}$ and $\phi_2^{(n)}$ (where $n=0, \ldots, N$) which are equal to $\mathcal{P}_1$ and $\mathcal{P}_2$ at $\eta=-1+(n/h)$, where $h=2/(N-1)$. Applying simple centered differencing to (4.8)–(4.9), we find

$$\begin{aligned}&[(\eta^{(n)}-1)h^2+\tfrac{1}{2}h]\phi_2^{(n+1)}\\&\quad+[-2h^2(\eta^{(n)}-1)-\mathrm{Ri}^2\mathrm{Ro}^2(\eta^{(n)}-1)-\tfrac{1}{2}\,\mathrm{Ri}]\phi_2^{(n)}\\&\quad+[(\eta^{(n)}-1)h^2-\tfrac{1}{2}h]\phi_2^{(n-1)}-\tfrac{1}{2}\,\mathrm{Ri}\phi_1^{(n)}\\&\quad-\tau\{[-(\eta^{(n)}-1)h^2-\tfrac{1}{2}h]\phi_2^{(n+1)}\\&\quad+[2h^2(\eta^{(n)}-1)+\mathrm{Ri}^2\mathrm{Ro}^2(\eta^{(n)}-1)-\tfrac{1}{2}\,\mathrm{Ri}]\phi_2^{(n)}\\&\qquad+[-(\eta^{(n)}-1)h^2+\tfrac{1}{2}h]\phi_2^{(n-1)}+\tfrac{1}{2}\,\mathrm{Ri}\phi_1^{(n)}\}=0,\end{aligned}\tag{A1}$$

$$\begin{aligned}&[(\eta^{(n)}+1)h^2+\tfrac{1}{2}h]\phi_1^{(n+1)}\\&\quad+[-2h^2(\eta^{(n)}+1)-\mathrm{Ri}^2\mathrm{Ro}^2(\eta^{(n)}+1)+\tfrac{1}{2}\,\mathrm{Ri}]\phi_1^{(n)}\\&\quad+[(\eta^{(n)}-1)h^2-\tfrac{1}{2}h]\phi_1^{(n-1)}-\tfrac{1}{2}\,\mathrm{Ri}\phi_2^{(n)}\\&\quad-\tau\{[(\eta^{(n)}+1)h^2+\tfrac{1}{2}h]\phi_1^{(n+1)}\\&\quad+[-2h^2(\eta^{(n)}+1)-\mathrm{Ri}^2\mathrm{Ro}^2(\eta^{(n)}+1)-\tfrac{1}{2}\,\mathrm{Ri}]\phi_1^{(n)}\\&\qquad+[(\eta^{(n)}+1)h^2-\tfrac{1}{2}h]\phi_1^{(n-1)}+\tfrac{1}{2}\,\mathrm{Ri}\phi_2^{(n)}\}=0,\end{aligned}\tag{A2}$$

where

$$\eta^{(n)}=-1+n/h,\quad n=1, 2, \ldots, N-2, N-1.$$

The finite-differenced form of the boundary conditions may be written

$$\begin{aligned}&-\tfrac{1}{2}h(1-\tau)\phi_1^{(2)}\\&\quad+[\tfrac{1}{2}h(4\phi_1^{(1)}-3\phi_1^{(0)})+\mathrm{Ri}(\phi_1^{(0)}+\phi_2^{(0)})/2]\\&\qquad-\tau[\tfrac{1}{2}h(4\phi_1^{(1)}-3\phi_1^{(0)})-\tfrac{1}{2}\,\mathrm{Ri}(\phi_1^{(0)}-\phi_2^{(0)})]=0,\end{aligned}\tag{A3}$$

$$-2h\phi_1^{(N-1)}+\tfrac{1}{2}\phi_1^{(N-2)}+(3h/2+\mathrm{RiRo})\phi_1^{(N)}=0,\tag{A4}$$

$$\begin{aligned}&-\tfrac{1}{2}h(1+\tau)\phi_2^{(N-2)}\\&\quad+[\tfrac{1}{2}h(4\phi_2^{(N-1)}-3\phi_2^{(N)})+\tfrac{1}{2}\,\mathrm{Ri}(\phi_2^{(N)}+\phi_1^{(N)})]\\&\quad-\tau[-\tfrac{1}{2}h(4\phi_2^{(N-1)}-3\phi_2^{(N)})-\tfrac{1}{2}\,\mathrm{Ri}(\phi_1^{(N)}-\phi_2^{(N)})]=0\end{aligned}\tag{A5}$$

$$2h\phi_2^{(1)}-\tfrac{1}{2}h\phi_2^{(2)}-(3h/2+\mathrm{RiRo})\phi_2^{(0)}=0.\tag{A6}$$

Although Eqs. (A1), (A2), (A3) and (A5) are linear in τ, the absence of τ from (A4) and (A6) precludes the solving of (A1)–(A6) as a linear eigenvalue problem in its present form.

To circumvent this difficulty, I used the equations found when $n=1$ and $N-1$ in (A1)–(A2) to form a set of eight equations [along with (A3)–(A6)] which describe $\phi_2^{(0)}$, $\phi_1^{(0)}$, $\phi_2^{(1)}$, $\phi_1^{(1)}$, $\phi_2^{(2)}$, $\phi_1^{(2)}$, $\phi_2^{(N-2)}$, $\phi_1^{(N-2)}$, $\phi_2^{(N-1)}$, $\phi_1^{(N-1)}$, $\phi_2^{(N)}$ and $\phi_1^{(N)}$. These equations can be reduced to four in number by algebraic manipulation to eliminate $\phi_2^{(2)}$, $\phi_1^{(2)}$, $\phi_2^{(N-2)}$ and $\phi_1^{(N-2)}$. These four equations may be further manipulated so that they have the form

$$\begin{aligned}&\{(4h^2(\eta^{(1)}-1)-2\,\mathrm{Ri}^2\mathrm{Ro}^2(\eta^{(1)}-1)-\mathrm{Ri}+4h][4h(\eta^{(1)}+1)-2\,\mathrm{Ri}^2\mathrm{Ro}^2(\eta^{(1)}+1)-\mathrm{Ri}+4h]-\mathrm{Ri}^2\}\phi_2^{(1)}\\&\quad+\{-\mathrm{Ri}[4h^2(\eta^{(1)}+1)-2\,\mathrm{Ri}^2\mathrm{Ro}^2(\eta^{(1)}+1)+4h]-\mathrm{Ri}[4h^2(\eta^{(1)}+1)-2\,\mathrm{Ri}^2\mathrm{Ro}^2(\eta^{(1)}+1)+4h]\}\phi_1^{(1)}\\&\quad+\{[-4(\eta^{(1)}-1)h^2-4h-4\,\mathrm{RiRo}(\eta^{(1)}-1)h-2\,\mathrm{RiRo}][4h^2(\eta^{(1)}+1)-2\,\mathrm{Ri}^2\mathrm{Ro}^2(\eta^{(1)}+1)-\mathrm{Ri}+4h]\\&\quad-\mathrm{Ri}^2[2(\eta^{(1)}+1)h+1]\}\phi_2^{(0)}+\mathrm{Ri}[4h^2(\eta^{(1)}+1)+4h-\mathrm{Ri}-2\,\mathrm{Ri}(\eta^{(1)}+1)h]\phi_1^{(0)}\\&\quad-\tau(\{[4h^2(\eta^{(1)}+1)-2\,\mathrm{Ri}^2\mathrm{Ro}^2(\eta^{(1)}+1)-\mathrm{Ri}+4h][-4h^2(\eta^{(1)}-1)+2\,\mathrm{Ri}^2\mathrm{Ro}^2(\eta^{(1)}-1)-\mathrm{Ri}-4h]-\mathrm{Ri}^2\}\phi_2^{(1)}\\&\quad+\{[4h^2(\eta^{(1)}-1)+4h+4\,\mathrm{RiRo}h(\eta^{(1)}-1)+2\,\mathrm{RiRo}][4h^2(\eta^{(1)}+1)-2\,\mathrm{Ri}^2\mathrm{Ro}^2(\eta^{(1)}+1)-\mathrm{Ri}+4h]\\&\qquad-\mathrm{Ri}^2[2(\eta^{(1)}+1)h+1]\}\phi_2^{(0)}+\mathrm{Ri}[4h^2(\eta^{(1)}+1)+4h+\mathrm{Ri}+2\,\mathrm{Ri}h(\eta^{(1)}+1)]\phi_1^{(0)})=0,\end{aligned}\tag{A7}$$

$$\begin{aligned}&[4h^2(\eta^{(1)}+1)-2\,\mathrm{Ri}^2\mathrm{Ro}^2(\eta^{(1)}+1)+4h+\mathrm{Ri}]\phi_1^{(1)}+\mathrm{Ri}\phi_2^{(1)}+[-4h^2(\eta^{(1)}+1)-4h+\mathrm{Ri}+2\,\mathrm{Ri}(\eta^{(1)}+1)h]\phi_1^{(0)}\\&\quad+[2(\eta^{(1)}+1)h+1]\,\mathrm{Ri}\phi_2^{(0)}-\tau\{[4h^2(\eta^{(1)}+1)-2\,\mathrm{Ri}^2\mathrm{Ro}^2(\eta^{(1)}+1)-\mathrm{Ri}+4\mathrm{h}]\phi_1^{(1)}+\mathrm{Ri}\phi_2^{(1)}\\&\qquad+[-4h^2(\eta^{(1)}+1)-4h-\mathrm{Ri}-2\,\mathrm{Ri}(\eta^{(1)}+1)h]\phi_1^{(0)}+\mathrm{Ri}[2(\eta^{(1)}+1)h+1]\phi_2^{(0)}\}=0,\end{aligned}\tag{A8}$$

$$\begin{aligned}&[-4h^2(\eta^{(N-1)}-1)+4h+\mathrm{Ri}(2(\eta^{(N-1)}-1)h-1)]\phi_2^{(N)}+\mathrm{Ri}[2(\eta^{(N-1)}-1)h-1]\phi_1^{(N)}\\&\quad+[4h^2(\eta^{(N-1)}-1)-2\,\mathrm{Ri}^2\mathrm{Ro}^2(\eta^{(N-1)}-1)-\mathrm{Ri}-4h]\phi_2^{(N-1)}-\mathrm{Ri}\phi_1^{(N-1)}\\&\quad-\tau\{[-4h^2(\eta^{(N-1)}-1)+2\,\mathrm{Ri}^2\mathrm{Ro}^2(\eta^{(N-1)}-1)-\mathrm{Ri}+4h]\phi_2^{(N-1)}+\mathrm{Ri}\phi_1^{(N-1)}\\&\qquad+[4h^2(\eta^{(N-1)}-1)-4h+2\,\mathrm{Ri}(\eta^{(N-1)}-1)h-\mathrm{Ri}]\phi_2^{(N)}-[2\,\mathrm{Ri}(\eta^{(N-1)}-1)h-\mathrm{Ri}]\phi_1^{(N)}\}=0,\end{aligned}\tag{A9}$$

$$\begin{aligned}&\{[4h^2(\eta^{(N-1)}+1)-4h+4\,\mathrm{RiRo}(\eta^{(N-1)}+1)h-2\,\mathrm{RiRo}][4h^2(\eta^{(N-1)}-1)-2\,\mathrm{Ri}^2\mathrm{Ro}^2(\eta^{(N-1)}-1)+\mathrm{Ri}-4h]\\&\quad-\mathrm{Ri}^2[2h(\eta^{(N-1)}-1)-1]\}\phi_1^{(N)}+\{[4h^2(\eta^{(N-1)}+1)-2\,\mathrm{Ri}^2\mathrm{Ro}^2(\eta^{(N-1)}+1)+\mathrm{Ri}-4h]\\&\quad\times[-4h^2(\eta^{(N-1)}-1)+2\,\mathrm{Ri}^2\mathrm{Ro}^2(\eta^{(N-1)}-1)-\mathrm{Ri}+4h]+\mathrm{Ri}^2\}\phi_1^{(N-1)}\\&\quad+\mathrm{Ri}[4h^2(\eta^{(N-1)}-1)-4h-2\,\mathrm{Ri}h(\eta^{(N-1)}-1)+\mathrm{Ri}]\phi_2^{(N)}\\&\quad+2\,\mathrm{Ri}[-4h^2(\eta^{(N-1)}-1)+2\,\mathrm{Ri}^2\mathrm{Ro}^2(\eta^{(N-1)}-1)+4h]\phi_2^{(N-1)}\\&\quad-\tau(\{[4h^2(\eta^{(N-1)}+1)-4h+4\,\mathrm{RiRo}h(\eta^{(N-1)}+1)-2\,\mathrm{RiRo}][4h^2(\eta^{(N-1)}-1)-2\,\mathrm{Ri}^2\mathrm{Ro}^2(\eta^{(N-1)}-1)\\&\quad+\mathrm{Ri}-4h]+\mathrm{Ri}^2[2(\eta^{(N-1)}-1)h-1]\}\phi_1^{(N)}+\{[4h^2(\eta^{(N-1)}+1)-2\,\mathrm{Ri}^2\mathrm{Ro}^2(\eta^{(N-1)}+1)-\mathrm{Ri}-4h]\\&\quad\times[-4h^2(\eta^{(N-1)}-1)+2\,\mathrm{Ri}^2\mathrm{Ro}^2(\eta^{(N-1)}-1)-\mathrm{Ri}+4h]-\mathrm{Ri}^2\}\phi_1^{(N-1)}\\&\qquad-\mathrm{Ri}[4h^2(\eta^{(N-1)}-1)-4h+2\,\mathrm{Ri}(\eta^{(N-1)}-1)h-\mathrm{Ri}]\phi_2^{(N)})=0.\end{aligned}\tag{A10}$$

Eqs. (A7)–(A10) along with (A1)–(A2) make up a system of $2N$ equations with $2N$ unknowns. Since all the equations are linear in τ, they may be written in the canonical format of

$$(A-\tau B)\mathbf{x}=\mathbf{0}, \tag{A11}$$

where A and B are matrices which contain the coefficients of the linear of equations, (A1)–(A2) and (A7)–(A10). These coefficients are stored in A and B in such a manner that $\mathbf{x}$, the eigenvector, is $(\phi_2^{(0)}, \phi_1^{(0)}, \phi_2^{(1)}, \phi_1^{(1)}, \ldots, \phi_2^{(N-1)}, \phi_1^{(N-1)}, \phi_2^{(N)}, \phi_1^{(N)})$. It should be further noted that (A7)–(A10) were derived with the explicit intention to make B a pentadiagonal matrix. Consequently, its inversion can be performed rapidly and with little core storage.

Therefore, upon computing the inverse of B, (A10) may be written

$$(B^{-1}A-\tau I)\,\mathbf{x}=\mathbf{0}, \tag{A12}$$

the canonical form of the classic linear eigenvalue problem. For a given Ro, Ri and N, the eigenvalues and eigenvectors may be found through the use of a number of well-known numerical methods; the numerical methods used are described in Appendix B.

APPENDIX B

Numerical Methods for Finding Eigenvectors and Eigenvalues

In this Appendix we shall describe the numerical techniques that were employed to solve (A10),

$$(A-B\tau)\mathbf{x}=\mathbf{0}. \tag{B1}$$

Our first task is to find the inverse of B so that (B1) may be rewritten in the canonical form

$$(B^{-1}A-\tau I)\mathbf{x}=\mathbf{0}. \tag{B2}$$

The inverse was found using Gaussian elimination with pivoting. Since B is pentadiagonal, its banded structure may be taken into account in preforming the Gaussian elimination, resulting in considerable saving of core storage and computational time.

After performing the matrix multiplication, the eigenvalue problem was solved using a series of sophisticated routines devised by Wilkinson *et al.* (1971).

First, the matrix $B^{-1}A$ is balanced through the use of routine BALANC (see Wilkinson and Reinsch, 1971, 315–326). The determination of an accurate eigensystem may present practical difficulties if the matrix is badly balanced, that is, if corresponding rows and columns have very different norms.

After balancing, the balanced $B^{-1}A$ is reduced to upper-Hessenberg form (a matrix such that $h_{ij}=0$ when $i>j+1$) by real stabilized elementary similarity transformations through the use of the routine ELMHES (see Wilkinson and Reinsch, 1971, 339–358). All of the eigenvalues of this transformed, real upper-Hessenberg matrix are then found through the use of the QR algorithm in a subroutine HQR (see Wilkinson and Reinsch, 1971, 359–371).

When the eigenvectors were needed, for example, to calculate the energetics, the eigenvectors for a specified eigenvalue were calculated by inverse iteration using the subroutine INVIT (see Wilkinson and Reinsch, 1971, 418–439). Before these eigenvectors could be used, however, the eigenvectors of the original matrix must be recovered from those of the balanced and transformed matrix using the procedures BALBAK and ELMBAK (see Wilkinson and Reinsch, 1971, 315–326 and 339–358).

REFERENCES

Charney, J. G., 1947: The dynamics of long waves in a baroclinic westerly current. *J. Meteor.*, **4**, 135–162.

Eady, E. T., 1949: Long waves and cyclonic waves. *Tellus,* **1**, 33–52.

Eliassen, A., 1949: The quasi-static equations of motion. *Geofys. Publ.*, **17**, No. 3.

Fjortøft, R., 1962: On the integration of a system of geostrophically balanced prognostic equations. *Proc. Intern. Symp. Numerical Weather Prediction*, Meteor. Soc. Japan, Tokyo, 153–159.

Hoskins, B. J., 1975: The geostrophic momentum approximation and semigeostrophic equations. *J. Atmos. Sci.*, **32**, 233–242.

——, 1976: Baroclinic waves and frontogenesis. Part I: Introduction and Eady wave. *Quart. J. Roy. Meteor. Soc.*, **102**, 130–122.

——, and F. P. Bretherton, 1972: Atmospheric frontogenesis models: Mathematical formulation and solution. *J. Atmos. Sci.*, **29**, 11–37.

Orlanski, I., 1968: Instability of frontal waves. *J. Atmos. Sci.*, **25**, 178–200.

Wilkinson, J. H., and C. Reinsch, 1971: *Handbook of Automatic Computation*, Vol. 2, *Linear Algebra*. Springer-Verlag, 439 pp.